Multistable chimera states in a smallest population of three coupled oscillators

A. Ragavan,[1] M. Manoranjani,[1] D. V. Senthilkumar,[2,*] and V. K. Chandrasekar[1,†]

[1]*Centre for Nonlinear Science & Engineering, School of Electrical & Electronics Engineering, SASTRA Deemed University, Thanjavur-613 401, Tamil Nadu, India*

[2]*School of Physics,Indian Institute of Science Education and Research, Thiruvananthapuram-695551, Kerala, India*

(Received 21 July 2022; revised 16 February 2023; accepted 28 March 2023; published 21 April 2023)

We uncover the emergence of distinct sets of multistable chimera states in addition to chimera death and synchronized states in a smallest population of three globally coupled oscillators with mean-field diffusive coupling. Sequence of torus bifurcations result in the manifestation of distinct periodic orbits as a function of the coupling strength, which in turn result in the genesis of distinct chimera states constituted by two synchronized oscillators coexisting with an asynchronous oscillator. Two subsequent Hopf bifurcations result in homogeneous and inhomogeneous steady states resulting in desynchronized steady states and chimera death state among the coupled oscillators. The periodic orbits and the steady states lose their stability via a sequence of saddle-loop and saddle-node bifurcations finally resulting in a stable synchronized state. We have generalized these results to N coupled oscillators and also deduced the variational equations corresponding to the perturbation transverse to the synchronization manifold and corroborated the synchronized state in the two-parameter phase diagrams using its largest eigenvalue. Chimera states in three coupled oscillators emerge as a solitary state in N coupled oscillator ensemble.

DOI: 10.1103/PhysRevE.107.044209

I. INTRODUCTION

The chimera state is a partially synchronized state, characterized by coexisting coherent and incoherent domains arising out of an ensemble of identical oscillators, which has attracted humongous attention for more than a decade. Kuramoto and Battogtokh first observed the intriguing behavior of coexisting domains of frequency entrained oscillators and oscillators with distributed frequencies in a network of nonlocally coupled phase oscillators in 2002 [1]. Later, in 2004 Abrams and Strogatz named it as a "chimera state" [2]. Since then, extensive investigations have been carried out in identifying distinct types of chimera state under various coupling configurations [3]. Initially, it was believed that nonlocal coupling is deemed to be a necessary condition for the onset of the chimera states. However, later investigations extended this phenomenon to global coupling [4,5], local coupling [6,7], star networks [8], time-varying coupling [9,10], and even more to hierarchical connections [11,12]. Further, chimera states are not specific to simple network topologies but are also found to manifest in a large class of complex networks including random and scale-free networks [13]. Chimera states have also been explored in two-dimensional [14,15], three-dimensional [16], and multilayer networks [17,18]. The investigations on chimera states have revealed distinct types of chimera states including amplitude chimera [19], amplitude mediated chimera [20], breathing chimera [21], traveling chimera [22], alternating chimera [23], itinerant chimera [24], imperfect chimera [25], spiral wave chimera [26], chimera death [41], and so on.

The genesis of chimera states is not just limited to an ensemble of oscillators. The notion of chimera has also been extended to a minimal network of oscillators and oscillator populations. Ashwin and Burylko proposed the notion of weak chimera, a type of invariant set, in a minimal network of coupled phase oscillators and suggested that weak chimeras may be responsible for organizing the dynamics of more general chimera states [27]. This work has seeded the momentum on investigations exploring the emergence of chimera states in smallest possible networks and their relevance to the genesis of more general chimera states. Chimera states are also found in two populations of two phase oscillators each with different interpopulation and intrapopulation coupling strengths [28]. It has also been shown that the bifurcations that facilitate the onset of chimera state in two smallest populations are similar to those observed in the continuum limit. Different types of chimera states such as local chimera, global chimera, amplitude chimera, and the multistability between them have also been shown in two populations of two oscillators each with the same inter- and intrapopulations coupling strengths but with a frequency mismatch between the populations [29]. Chimera states have also been reported in globally coupled three oscillators entitled smallest chimera states [30]. Interestingly, the coexisting state where one of the two symmetrically coupled identical oscillators settled at nearly periodic oscillation and the other at chaotic oscillation has also been reported as a chimera state [31]. Remarkably, smallest chimera states have also been reported experimentally in coupled pendula [25,29,32], optoelectronic oscillators [5], and semiconductor lasers [33–35].

In this paper, we consider $N = 3$ globally coupled oscillators with a mean-field diffusive coupling and unravel the emergence of distinct chimera states, chimera death state, and synchronized state along with a glossary of multistable

*Corresponding author: skumar@iisertvm.ac.in
†Corresponding author: chandru25nld@gmail.com

states among them. We elucidate a rich variety of bifurcation transitions as a function of the coupling strength using the one-parameter bifurcation diagrams. In particular, three successive torus bifurcations lead to the manifestation of three distinct stable periodic orbits from quasiperiodic oscillations, which in turn lead to the genesis of three distinct chimera states. Here, the chimera states are comprised of two synchronized oscillators coexisting with an asynchronous oscillator. Further, the onset of a homogeneous stable steady state via a Hopf bifurcation in a certain range of the coupling strength results in desynchronized steady states among the coupled systems. Furthermore, the onset of a second stable steady state, resulting in inhomogeneous steady states, via a second subsequent Hopf bifurcation leads to the manifestation of a chimera death state, where two oscillators populate the same steady state while the third oscillator populates a different steady state. Eventually, the periodic orbits and the steady states lose their stability subsequently via a sequence of saddle-loop and saddle-node bifurcations as the coupling strength is increased further finally resulting in the synchronized state. Different sets of the observed dynamical states coexists in different ranges of the coupling strength bounded by distinct bifurcation scenarios. We show a rich variety of multistable states among the observed collective dynamical states in the two-parameter phase diagrams. We also deduce the variational equations corresponding to the perturbation transverse to the synchronization manifold in N coupled oscillators and corroborate the region of synchronized state in the two-parameter phase diagrams using its largest Lyapunov exponent (master stability function). Interestingly, the chimera states in the $N = 3$ oscillator population emerge as distinct solitary states in $N = 100$ oscillator population via similar bifurcation transitions as in $N = 3$ population. The governing equation of motion corresponding to the solitary state with appropriately perturbed initial conditions results in a stable solitary state.

The plan of the paper is as follows. In Sec. II, we provide a brief discussion on the model that we have considered. In Sec. III, we discuss the emergent collective dynamical states, namely four distinct chimera states along with a synchronized state and multistabilities among them by numerically solving the coupled oscillators. In Sec. IV, we discuss the dynamical transitions in the two-parameter phase diagrams. In Sec. V, we extend our analysis to $N = 100$ coupled oscillators to generalize the observed results. Finally, we summarize our results in Sec. VI.

II. MODEL

We consider the following system of N globally coupled Rössler-like oscillators coupled via the mean-field diffusive coupling represented as

$$\dot{x}_i = -\omega_0\big(1 - \alpha\big(x_i^2 + y_i^2\big)\big)y_i - z_i + \epsilon(X - x_i), \tag{1a}$$

$$\dot{y}_i = \omega_0\big(1 - \alpha\big(x_i^2 + y_i^2\big)\big)x_i + ay_i, \tag{1b}$$

$$\dot{z}_i = b + (x_i - c)z_i, \tag{1c}$$

where $X = 1/N\sum_{i=1}^{N} x_i$, ω_0 is the natural frequency, α is the nonisochronocity parameter, and a, b, and c are the system parameters. The uncoupled systems are the paradigmatic Rössler systems when $\alpha = 0$. The role of nonisochronocity parameter α on the dynamics of the uncoupled and coupled Rössler-like system has been reported in detail in Ref. [36]. The Rössler-like system has been employed earlier to demonstrate phase-flip transition [37]. Mechanism for intensity-induced chimera states in globally coupled oscillators has also been explored using the Rössler-like system [38]. The presence of intensity-dependent self-interaction terms in the Rössler-like system results in increase in the number of fixed points and consequently multistable attractors in the phase space thereby resulting in the coexistence of distinct collective states based on the initial conditions. Suppression of chaos through coupling to an external chaotic system has been reported using the Rössler-like system [39]. Chimera states in the star network of Rössler-like system have also been reported by Meena *et al.* [8].

III. NUMERICAL RESULTS

We limit $N = 3$ coupled oscillators to elucidate the emergence of a rich variety of chimera states in the smallest possible network. We numerically solve the coupled oscillators (1) using the Runge-Kutta fourth-order integration scheme with a step size of $h = 0.01$. The natural frequency is fixed as $\omega_0 = 1.0$ and the nonisochronocity parameter as $\alpha = 0.01$. Other parameters are fixed as $a = 0.2$, $b = 1.7$, and $c = 5.7$. We start with analyzing one-parameter bifurcation diagrams and the involved dynamical transitions. One-parameter bifurcation diagrams, obtained using XPPAUT [40], are depicted in Fig. 1 in four different ranges of the coupling strength to view the bifurcation transitions clearly. Unfilled symbols correspond to unstable periodic orbits. Lines connected by filled symbols correspond to stable periodic orbits. Dashed and solid lines correspond to unstable and stable steady states. Vertical dotted-dashed lines demarcate distinct collective dynamical regions.

One-parameter bifurcation diagram in the range of $\varepsilon \in [0, 0.12]$ is depicted in Fig. 1(a). Unstable periodic orbits become stable periodic orbits through a successive torus bifurcations. Unstable synchronized oscillatory state (unfilled diamonds) manifests as a stable synchronized oscillatory state (lines connected by filled diamonds) for a sufficiently large coupling strength [see Fig. 1(d)]. The stable quasiperiodic oscillation coexisting with the unstable periodic orbit, indicated by unfilled circles, loses its stability via a torus bifurcation T_1 at $\varepsilon = 0.072$ [see Fig. 1(b)] giving rise to a stable periodic oscillation, indicated by the line connected by filled circles. The quasiperiodic oscillation accompanied by the unstable periodic orbit, indicated by unfilled triangles, loses its stability via a second torus bifurcation T_2 at $\varepsilon = 0.1$ giving rise to a stable periodic oscillation, indicated by the line connected by filled triangles. Similarly, the quasiperiodic oscillation coexists along with the unstable periodic orbit, indicated by unfilled squares, loses its stability via a third torus bifurcation T_3 at $\varepsilon = 0.15$ [see Fig. 1(b)] giving rise to a stable periodic oscillation, indicated by the line connected by filled squares. Unstable steady states (indicated by dashed and dotted lines) manifest as stable steady states (indicated by solid black and

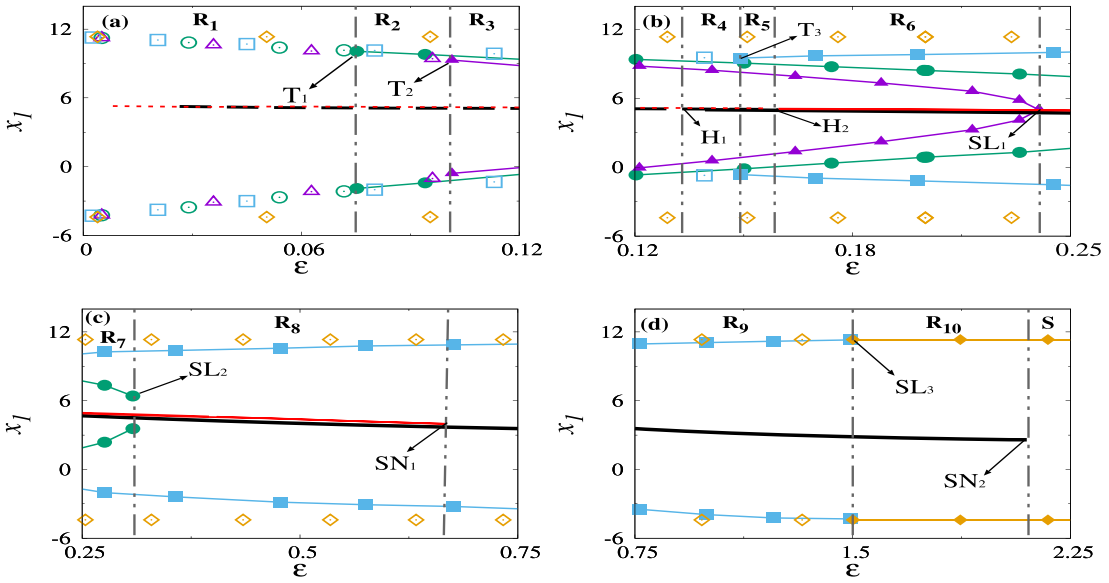

FIG. 1. One-parameter bifurcation diagrams, obtained using XXPAUT software, elucidating the dynamical transitions in different ranges of the coupling strength. (a) $\varepsilon \in (0, 0.12]$, (b) $\varepsilon \in [0.12, 0.25]$, (c) $\varepsilon \in [0.25, 0.75]$, and (d) $\varepsilon \in [0.75, 2.25]$. Unfilled circles, triangles, squares correspond to unstable periodic orbits that become stable periodic orbits, lines connected by filled symbols, through successive torus bifurcations. The unfilled diamonds correspond to unstable synchronized oscillatory state which gives rise to stable synchronized oscillatory state for a sufficiently large coupling strength. Dashed and solid lines correspond to unstable and stable steady states.

red lines) via the Hopf bifurcations H_1 at $\varepsilon = 0.14$ and H_2 at $\varepsilon = 0.155$ [see Fig. 1(b)].

The time traces of the periodic orbits of the uncoupled Rössler-like oscillators (1) for the above choice of parameters are depicted in Fig. 2(a). It is evident from the figure that all the three oscillators evolve independent of each other. Three different quasiperiodic oscillations of all the three oscillators are depicted in Figs. 2(b)–2(d) for $\varepsilon = 0.02, 0.04$, and 0.05, respectively, for appropriate initial conditions. The insets in Figs. 2(b) and 2(d) are shown to elucidate that the oscillators indeed evolve independently on the quasiperiodic orbits without any correlations. The desynchronized quasiperiodic oscillations in Figs. 2(b)–2(d) are denoted as D1, D2, and D3, respectively. All the three distinct quasiperiodic oscillations coexist in the region R_1 of the one-parameter bifurcation diagram [see Fig. 1(a)] in the range of the coupling strength $\varepsilon \in (0.0, 0.072)$. All the oscillators evolve asynchronously in the region R_1. However, there is a manifestation of a stable periodic orbit in all the three oscillators due to the torus bifurcation T_1 at $\varepsilon = 0.072$ and as a consequence multistable states emerge in the region R_2 in the range $\varepsilon \in [0.072, 0.1)$. In particular, one can observe desynchronized states of quasiperiodic oscillations D2 and D3 and chimera state C1 depending on the choice of initial conditions. The chimera state C1 is illustrated in Fig. 3(a) for $\varepsilon = 0.2$, where two oscillators are synchronized to the same stable periodic orbit while the third oscillator evolves independently on a different periodic orbit. Note that each oscillator has a distinct stable periodic orbit due to T_1. We coined the dynamical state depicted in Fig. 3(a) as a chimera state in the same vein as reported in Ref. [29]. It is to be noted that the coherent and incoherent domains constituting the chimera state reported by Maistrenko *et al.* in Ref. [29] has distinct frequencies. However, here it is evident from Fig. 3(a) that the coherent and incoherent domains are oscillations with clearly distinct amplitudes constituting amplitude chimera. The distinct chimeras reported in this paper are indeed amplitude chimeras [41–43], which are hereafter referred to as simply chimera throughout the paper. Analogously, stable chimera characterized by distinct phases but with the same frequency of the phase oscillators has also been reported [44,45]. The chimera state reported here can also be viewed as a solitary state [46–50]. C1, D2, and D3 coexists in the region R_2.

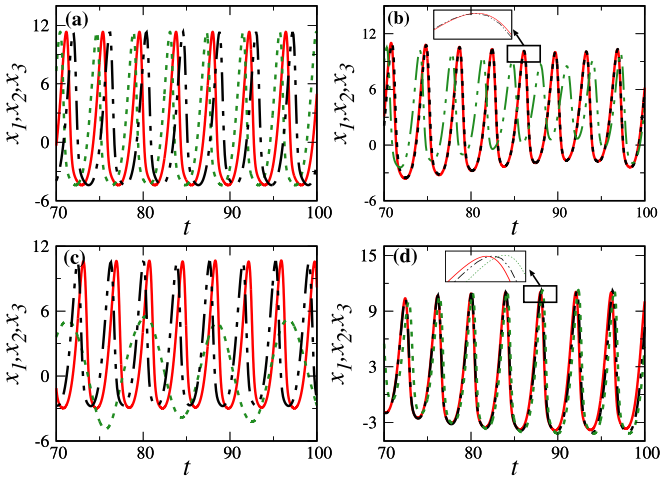

FIG. 2. The time traces of the three coupled Rössler-like oscillators (1), depicted using three different line types, for different values of the coupling strength. (a) Periodic orbit for $\varepsilon = 0.0$, (b) Desynchronized quasiperiodic states (D1) for $\varepsilon = 0.02$, (c) Desynchronized quasiperiodic states (D2) for $\varepsilon = 0.04$, and (d) Desynchronized quasiperiodic states (D3) for $\varepsilon = 0.05$.

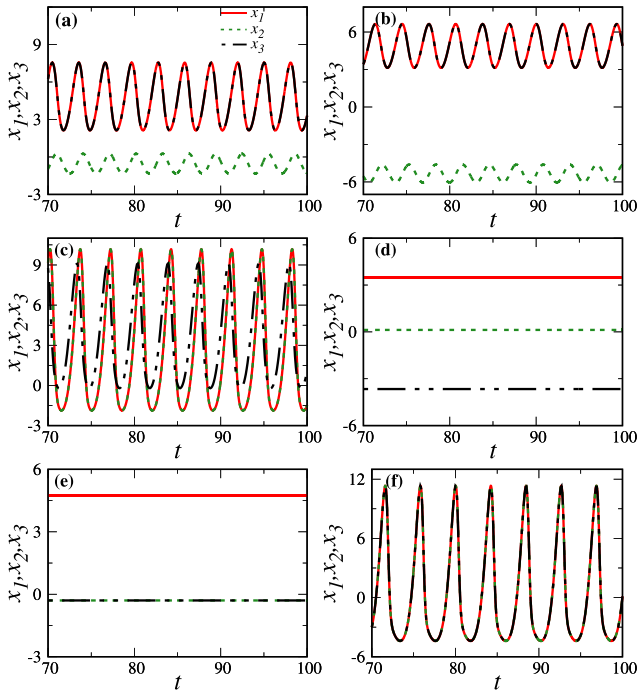

FIG. 3. The time traces of the three coupled Rössler-like oscillators (1), depicted using three different line types, for different values of the coupling strength. (a) Chimera state (C1) for $\varepsilon = 0.2$, (b) chimera state (C2) for $\varepsilon = 0.2$, (c) chimera state (C3) for $\varepsilon = 0.2$, (d) desynchronized steady states (D4) for $\varepsilon = 0.4$, (e) chimera death state (C4) for $\varepsilon = 0.4$, and (f) synchronized state (S) for $\varepsilon = 2.5$.

In the region R_3, in the range $\varepsilon \in [0.1, 0.15)$, there emerges a chimera state C2 in addition to the chimera state C1 at the cost of D2 due to the torus bifurcation T_2 at $\varepsilon = 0.1$. Consequently, C1, C2, and D3 coexists in the region R_3. The chimera state C2, characterized by two synchronized oscillators evolving on the same periodic orbit and a desynchronized oscillator evolving on a different periodic orbit, is depicted in Fig. 3(b) for $\varepsilon = 0.2$. The Hopf bifurcation H_1 at $\varepsilon = 0.14$ switches the unstable steady state (indicated by dashed line) to a stable steady state (solid black line). Hence in the region R_4 [see Fig. 1(b)], enclosed between the Hopf bifurcation H_1 and the torus bifurcation T_3 in the range $\varepsilon \in [0.14, 0.15)$, one can observe additional desynchronized steady states, represented as D4, [see Fig. 3(d) depicted for $\varepsilon = 0.4$], where all the three oscillators populate different steady states. The chimera states C1 and C2, and the desynchronized states D3 and D4 coexist in the region R_4. Third torus bifurcation at $\varepsilon = 0.15$ results in a third stable periodic orbit for each oscillator and consequently, chimera state C3 emerges at T_3. The chimera state C3 is depicted in Fig. 3(c) for $\varepsilon = 0.2$. Chimera states C1, C2, and C3, and the desynchronized state D4 coexist in the multistable region R_5 enclosed by the torus bifurcation T_3 and the second Hopf bifurcation H_2 in the range of $\varepsilon \in [0.15, 0.155)$ [see Fig. 1(b)].

The second Hopf bifurcation H_2 at $\varepsilon = 0.155$ switches the unstable steady state (indicated by dotted line) to stable steady state (solid red line). As a consequence, one can observe a chimera death state, represented as C4, where two oscillators populate the same steady state while the third oscillator populate a different steady as depicted in Fig. 3(e) for $\varepsilon = 0.4$. Chimera states C1, C2, and C3, chimera death state C4 and the desynchronized state D4 coexist in the region R_6 enclosed by the Hopf bifurcation HB_2 and a saddle-loop bifurcation SL_1 in the range of $\varepsilon \in [0.155, 0.23)$ [see Figs. 1(b) and 1(c)]. Note that one of the three periodic orbits, appeared via T_2, loses its stability via the saddle-loop bifurcation SL_1 at $\varepsilon = 0.23$ and consequently, the chimera state C2 loses its stability. Hence, in the region R_7 enclosed by the saddle-loop bifurcations SL_1 and SL_2 in the range of $\varepsilon \in [0.23, 0.31)$, the collective states C1, C3, C4, and D4 coexist. Further, one of the two stable periodic orbits, appeared via T_1, loses its stability at the second saddle-loop bifurcation SL_2 at $\varepsilon = 0.31$ resulting in destabilization of the chimera state C1. Hence, the multistable states C3, C4, and D4 coexist in the region R_8 bounded by the saddle-loop bifurcation SL_2 and a saddle-node bifurcation SN_1 [see Fig. 1(c)]. The stable steady state appeared via the Hopf bifurcation H_2 loses its stability via a saddle-node bifurcation SN_1 at $\varepsilon = 0.785$ and as a consequence the chimera death state C4 loses its stability simultaneously at SN_1. Hence, only C3 and D4 coexists in the region R_9 in the range of $\varepsilon \in [0.785, 1.5)$. Furthermore, the stable periodic orbit, appeared via T_3, loses its stability via a third saddle-loop bifurcation SL_3, and as a result the chimera state C3 also loses its stability. However, the unstable synchronized periodic orbit, indicated by unfilled diamond, attains stability simultaneously at SL_3. Consequently, the synchronized state, denoted by S, coexists with the desynchronized steady states D4 in the region R_{10} in the range of $\varepsilon \in [1.5, 2.11)$ [see Figs. 1(c) and 1(d)]. The steady state, stabilized via H_1, is destabilized via a second saddle-node bifurcation SN_2 at $\varepsilon = 2.11$ and hence the synchronized state alone persists for $\varepsilon \geqslant 2.11$. The time trace of the synchronized state is depicted in Fig. 3(f) for $\varepsilon = 2.5$

IV. GLOBAL DYNAMICAL TRANSITIONS

Two-parameter bifurcation diagrams are depicted in Fig. 4 in the (ε, α) parameter space for different ranges of the coupling strength as in the one-parameter bifurcation diagrams to elucidate the global dynamical transitions clearly. The nonisochronocity parameter is varied in the range $\alpha \in (0, 0.02)$ in all the four two-parameter phase diagrams. Distinct multistable regions, R_1 to R_{15}, are depicted with different color shades along with their boundaries. The multistable regions R_1 to R_{10} are exactly the same as depicted and discussed in the one-parameter bifurcation diagrams (see Figs. 1). Two-parameter bifurcation diagram in the range of $\alpha \in (0.0, 0.12]$ is depicted in Fig. 4(a). For $\alpha \approx (0.0, 0.012)$, there is a transition from R_1 to synchronized oscillatory state in depicted range of the coupling strength. There is a transition from R_1 to R_{15} (multistable region among D4, C4, and S) in the range of $\alpha \approx [0.012, 0.15)$ as a function of ε. Transition from R_1 to R_2, R_1 to R_3 via R_2, R_1 to R_3, R_1 to R_3 via R_{11} (multistable region among C2, D1, and D3), R_1 to R_{11}, and R_1 to R_{12} (multistable region among C2, C3, and D1) via R_{11}, are observed sequentially in appropriate ranges of the nonisochronocity parameter as a function of the coupling strength.

Two-parameter bifurcation diagram in the range of $\alpha \in [0.12, 0.24]$ is depicted in Fig. 4(b). Synchronized state and

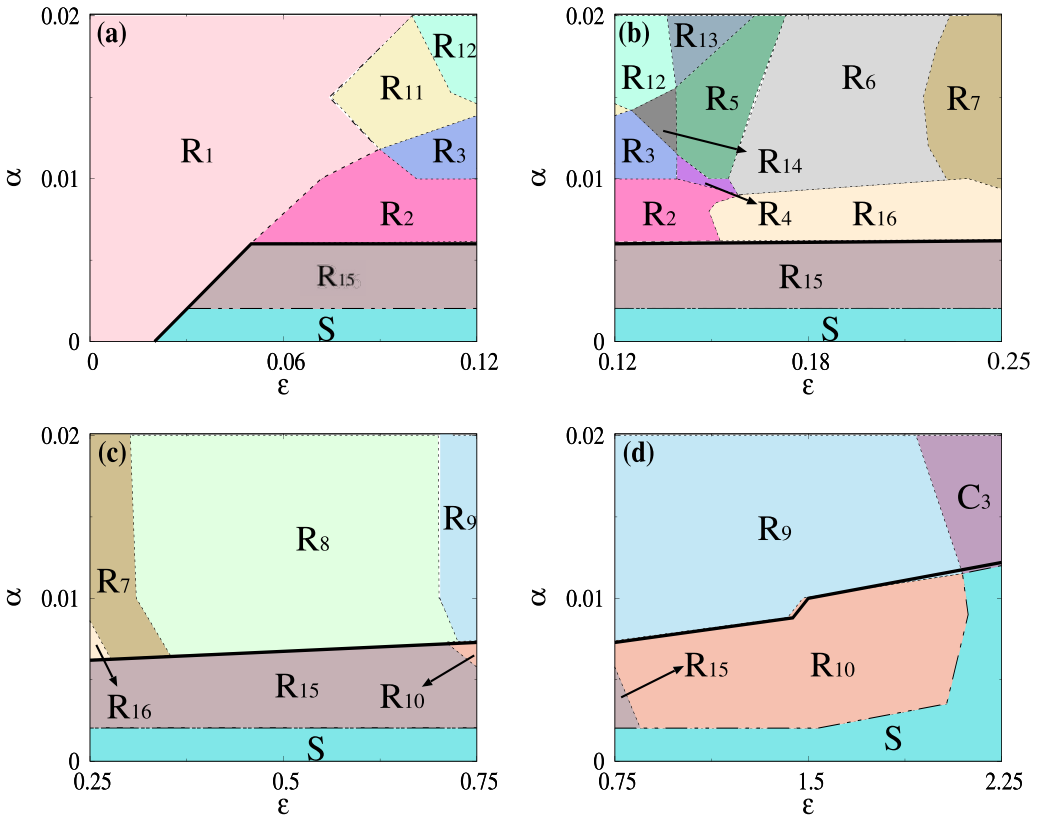

FIG. 4. Two-parameter phase diagrams in the (ε, α) parameter space. The nonisochronocity parameter is varied in the range $\alpha \in (0, 0.02)$ in all the four two-parameter bifurcation diagrams. (a) $\varepsilon \in (0, 0.12]$, (b) $\varepsilon \in [0.12, 0.25]$, (c) $\varepsilon \in [0.25, 0.75]$, and (d) $\varepsilon \in [0.75, 2.25]$. Refer text for the details on the distinct collective dynamical states comprising the distinct multistable regions R_1 to R_{16}.

the multistable region R_{15} is observed in the entire explored range of ε in the same range of α as in Fig. 4(a). The multistable regions R_2-R_7 and R_{12}-R_{16} are observed in the two phase diagram [see Fig. 4(b)] as domains of various sizes and shapes. The multistable region R_{12} has coexisting C2, C3, and D1 states, while the states C2, C3, and D3 coexist in R_{13}. Similarly, multistability between C1, C2, C3, and D4 are observed in R_{14} and that between C2, C3, C4, and D4 are observed in R_{16}. Synchronized state and the multistable region R_{15} emerges for small values of α in the range of $\varepsilon \in [0.25, 0.75]$ [see Fig. 4(c)]. The multistable region R_8 occupies a large region of the parameter space in the two phase diagram. The region R_7 extends from Fig. 4(b) to Fig. 4(c) to a small range of ε. The region R_9 forms the rightmost boundary in Fig. 4(c) for larger values of α, which occupies a large region of the parameter space in the two-parameter phase diagram in Fig. 4(d) in the range of $\varepsilon \in [0.75, 2.25]$. Synchronized state, monostable region C3, multistable regions R_{10} and R_{15} are also observed in appropriate domains in the two-parameter phase diagram.

V. COLLECTIVE DYNAMICAL STATES OF N COUPLED OSCILLATORS AND THEIR STABILITY

In this section, we extend our investigation to $N = 100$ coupled oscillators and explore whether the observed dynamical states in $N = 3$ coupled oscillators can also manifest in a large collection of oscillators. At first, we deduce the variational equations for the synchronized state $(x_i = x, y_i = y, z_i = z)$, $i = 1, \ldots, N$ using the celebrated master stability formalism. The perturbations to the synchronized state of all the N oscillators can be represented as $(x_i = x + \eta_i, y_i = y + \xi_i, z_i = z + \zeta_i)$, where η_i, ξ_i, and ζ_i are very small perturbations to the i-th oscillator. The evolution equations corresponding to the perturbations can be obtained as

$$\begin{aligned}
\dot{\eta}_i &= -\omega_0(\xi_i - \alpha(x^2 + 3y^2)\xi_i - \alpha 2xy\eta_i) \\
&\quad - \zeta_i + \frac{\epsilon}{N}\sum_{k=1}^{N}(\eta_k - \eta_i), \\
\dot{\xi}_i &= \omega_0(\eta_i - \alpha(3x^2 + y^2)\eta_i - \alpha 2xy\xi_i) + a\xi_i, \\
\dot{\zeta}_i &= x\zeta_i + z\eta_i - c\zeta_i.
\end{aligned}$$

Now, with the transformation $(\eta, \xi, \zeta) = (\sum_{j=1}^{N}\eta_j, \sum_{j=1}^{N}\xi_j, \sum_{j=1}^{N}\zeta_j)$, the evolution equations for the perturbations parallel to the synchronization manifold can be written as

$$\begin{aligned}
\dot{\eta} &= -\omega_0(\xi - \alpha(x^2 + 3y^2)\xi - \alpha 2xy\eta) - \zeta, \\
\dot{\xi} &= \omega_0(\eta - \alpha(3x^2 + y^2)\eta - \alpha 2xy\xi) + a\xi, \\
\dot{\zeta} &= x\zeta + z\eta - c\zeta.
\end{aligned}$$

Note that the transformations correspond to the eigenvectors of the evolution equations for the perturbations corresponding to the zero eigenvalue. The evolution (variational) equations for the perturbations transverse to the synchronization

manifold can be obtained as

$$\dot{\eta}^k = -\omega_0(\xi^k - \alpha(x^2+3y^2)\xi^k - \alpha 2xy\eta^k) - \zeta^k - \epsilon\eta^k,$$
$$\dot{\xi}^k = \omega_0(\eta^k - \alpha(3x^2+y^2)\eta^k - \alpha 2xy\xi^k) + a\xi^k,$$
$$\dot{\zeta}^k = x\zeta^k + z\eta^k - c\zeta^k,$$

where $(\eta^k, \xi^k, \zeta^k) = (\eta_k - \eta_1, \xi_k - \xi_1, \zeta_k - \zeta_1)$, $k = 2, 3, \ldots N$. The eigenvalues of the variational equations determine the stability of the synchronized state. The synchronization manifold is stable if the largest eigenvalue of the variational equations is negative and it will be unstable even if one of the eigenvalues turnout to be positive. The above stability criterion is valid for any N and consequently the region of stable synchronized state in the two-parameter phase diagrams (see Fig. 4) for $N = 3$ is also corroborated from the largest eigenvalue of the corresponding variational equations. In particular, the stable synchronized regions below the solid black lines in Figs. 4 are also corroborated from the value of the largest eigenvalue of the variational equations.

It is to be noted that the chimera states in $N = 3$ coupled oscillators manifest as a solitary state for $N > 3$. Note that only one of the oscillators evolves asynchronously from the rest of two synchronized oscillators constituting chimera state for $N = 3$. Analogously, choosing $N - 1$ oscillators as synchronous oscillators and Nth as asynchronous one for the case of N oscillators, the resulting self-organizing dynamics turns out to be a solitary state. The evolution equations for the $N - 1$ synchronized oscillators can be represented as

$$\dot{x}_s = -\omega_0\big[1 - \alpha\big(x_s^2 + y_s^2\big)\big]y_s - z_s + \hat{\epsilon}(x_d - x_s), \quad (2a)$$
$$\dot{y}_s = \omega_0\big[1 - \alpha\big(x_s^2 + y_s^2\big)\big]x_s + ay_s, \quad (2b)$$
$$\dot{z}_s = b + (x_s - c)z_s, \quad (2c)$$

and that corresponding to the desynchronized oscillator can be written as

$$\dot{x}_d = -\omega_0\big[1 - \alpha\big(x_d^2 + y_d^2\big)\big]y_d - z_d + (N-1)\hat{\epsilon}(x_s - x_d),$$
$$\dot{y}_d = \omega_0\big[1 - \alpha\big(x_d^2 + y_d^2\big)\big]x_d + ay_d,$$
$$\dot{z}_d = b + (x_d - c)z_d,$$

which together constitute the evolution equations corresponding to the solitary state [46–50]. Here for convenience we represent $\frac{\epsilon}{N}$ as $\hat{\epsilon}$.

The one-parameter bifurcation diagrams of the evolution equations corresponding to the synchronized oscillators, obtained using the XPPAUT software, are depicted in Figs. 5(a) and 5(b) in the range of the coupling strength $\hat{\epsilon} \in [0, 0.1)$ and $\hat{\epsilon} \in [0.1, 1.1]$, respectively. The symbols are similar to those discussed in Fig. 1. Only quasiperiodic oscillations are observed in the range of $\hat{\epsilon} \in [0, 0.005)$. Three torus bifurcations at T_1, T_2, and T_3 result in three stable periodic orbits as observed in Fig. 1 for $N = 3$ oscillators. Consequently, $N - 1$ oscillators have a stable synchronized periodic orbit in the range of $\hat{\epsilon} \in [0.005, 0.075)$, while the Nth oscillator evolve independently (which is not depicted here) constituting the solitary state S_1, a monostable state in the range of $\hat{\epsilon} \in [0.005, 0.075)$. The second torus bifurcation T_2 at $\hat{\epsilon} = 0.075$ results in a distinct stable synchronized periodic orbit in the range of $\hat{\epsilon} \in [0.075, 0.25)$ leading to a distinct solitary state

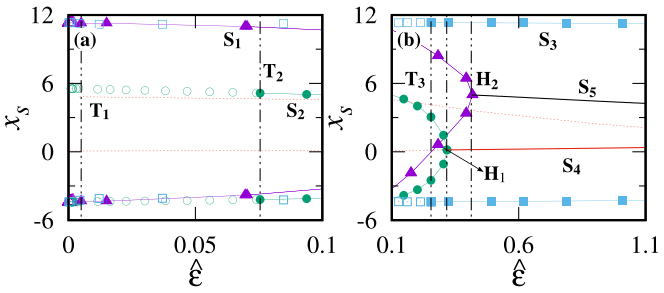

FIG. 5. One-parameter bifurcation diagrams of the evolution equation (2) corresponding to the $N - 1$ synchronized oscillators, obtained using XXPAUT software, elucidating the dynamical transitions in different ranges of the coupling strength (a) $\hat{\epsilon} \in [0, 0.1]$ and (b) $\hat{\epsilon} \in [0.1, 1.1]$. The symbols are similar to those discussed in Fig. 1.

S_2. Note that both S_1 and S_2 coexist in the latter range of the coupling strength due to the two distinct stable periodic orbits available for the $N - 1$ oscillators. The third torus bifurcation T_3 at $\hat{\epsilon} = 0.25$ results in the third stable periodic orbit and consequently the solitary state S_3. The stable periodic orbit manifested by T_2 loses its stability via a Hopf bifurcation H_1 at $\hat{\epsilon} = 0.31$ resulting in a stable synchronized steady state for $\hat{\epsilon} \geqslant 0.31$ (indicated by red solid line) leading to the onset of the fourth solitary state S_4. S_1, S_2, and S_3 coexist in the range of $\hat{\epsilon} \in [0.25, 0.31)$. Similarly, the stable periodic orbit manifested by T_1 loses its stability via a second Hopf bifurcation H_2 at $\hat{\epsilon} = 0.41$ resulting in a second stable synchronized steady state for $\hat{\epsilon} \geqslant 0.41$ (indicated by black solid line) leading to the emergence of fifth solitary state S_5. S_1, S_3 and S_4 coexist in the range of $\hat{\epsilon} \in [0.31, 0.41)$, while S_3, S_4, and S_5 coexist in the range of $\hat{\epsilon} \in [0.41, 1.1)$.

The spatiotemporal plot of the solitary state S_1 is depicted in Fig. 6(a) $\hat{\epsilon} = 0.35$. The synchronized domain is a synchronized oscillatory state, while the state of the independently evolving asynchronous oscillator is also an oscillatory state oscillating with a very small amplitude of oscillation. Note that the initial conditions for the $N - 1$ oscillators are randomly perturbed synchronized state (x_s, y_s, z_s) and that for the Nth oscillator is the perturbed state of (x_d, y_d, z_d) [see Fig. 6(b)] to realize the solitary state from the N coupled oscil-

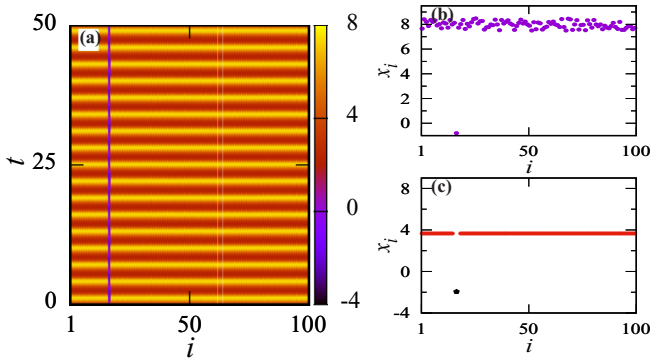

FIG. 6. Solitary state S_1 for $N = 100$ coupled oscillators for $\hat{\epsilon} = 0.35$. (a) Spatiotemporal plot, (b) distribution of initial conditions, and (c) snapshot of the spatiotemporal plot.

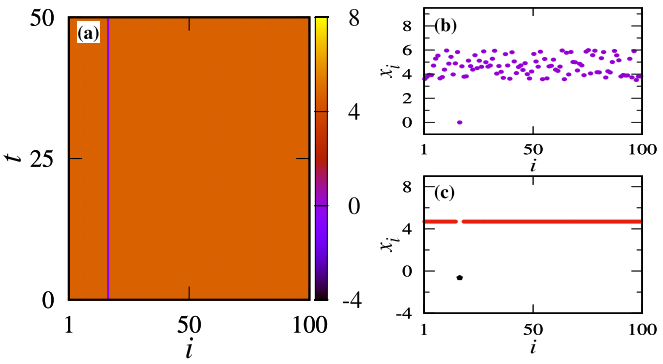

FIG. 7. Solitary state S_5 for $N = 100$ coupled oscillators for $\hat{\varepsilon} = 0.8$. (a) Spatiotemporal plot, (b) distribution of initial conditions, and (c) snapshot of the spatiotemporal plot.

lators. The snapshot of the spatiotemporal plot of the solitary state S_1 is depicted in Fig. 6(c). The spatiotemporal plot of the solitary state S_5 is depicted in Fig. 7(a) $\hat{\varepsilon} = 0.8$, where the synchronized state is a stable steady state induced by the Hopf bifurcation H_2 [see Fig. 5(b)] and the independently evolving asynchronous oscillator is also in its steady state. The perturbed initial conditions from the synchronized state is depicted in Fig. 7(b) and the snapshot of the solitary state S_5 is depicted in Fig. 7(c). We refrain from providing the spatiotemporal plots of other solitary state to avoid redundancy.

VI. SUMMARY AND CONCLUSIONS

We have considered a smallest population of three globally coupled Rössler-like oscillators with the mean-field diffusive coupling. We have unraveled distinct types of chimera states including chimera death and synchronized states as the coupling strength is varied. In particular, there exists a rich variety of distinct sets of multistability among the observed collective dynamical states in different ranges of the coupling strength bounded by distinct set of bifurcation scenario. There exist three distinct quasiperiodic orbits for small coupling strengths, which eventually manifest as stable periodic orbits through successive torus bifurcations. The three distinct periodic orbits lead to the genesis of three different chimera states, which coexist with desynchronized quasiperiodic oscillatory states in appropriate ranges of the coupling strength. The chimera state is characterized by the coexistence of two synchronized periodic oscillators and an asynchronous periodic oscillator. Further, two unstable steady states are stabilized via two subsequent Hopf bifurcations, which results in the manifestation of desynchronized steady states due to the homogeneous steady state, and chimera death state due to the onset of inhomogeneous steady states. The chimera death state is constituted by two oscillators that populate the same steady state while the third oscillator populates a different steady state, which we observe in the smallest population of three coupled oscillators. The periodic orbits and the steady states lose their stability through a sequence of saddle-loop and saddle-node bifurcations resulting in the synchronized state as the only stable state for large coupling strengths in the one parameter bifurcation diagram. Different sets of multistability among the observed dynamical states are found in the distinct ranges of the coupling strength bounded by distinct bifurcations. Two-parameter phase diagrams exhibit a rich variety of multistable states.

We have also extended our investigation for $N = 100$ oscillators to generalize the observed dynamical states. Interestingly, we found that the chimera state in three coupled oscillators emerges as the solitary states in an ensemble of oscillators with $N > 3$. We have deduced the variational equations corresponding to the perturbation transverse to the synchronization manifold using the master stability formalism and corroborated the synchronized state in the two-parameter phase diagrams using its largest eigenvalue. We have also pointed out that one can have distinct types of solitary states depending on the periodic attractors and the steady states. We strongly believe that the results of this paper enrich our knowledge on the admissible collective dynamical states and a rich variety of multistable states even in a smallest population of three coupled oscillators. Moreover, chimera states are found to have strong resemblance to the neural patterns and hence the multistable chimera states observed in this paper may form the basis for the cognitive behavior of the brain.

ACKNOWLEDGMENTS

The authors acknowledge the anonymous referees for their insightful comments, which greatly helped us to improve the manuscript. A.R. acknowledges the infrastructural support of SASTRA University. The work of V.K.C. is supported by the DST-CRG Project under Grant No. CRG/2020/004353 and DST, New Delhi for computational facilities under the DST-FIST program (SR/FST/PS- 1/2020/135) to the Department of Physics. D.V.S. is supported by the DST-SERB-CRG Project under Grant No. CRG/2021/000816. M.M. thanks the Department of Science and Technology, Government of India, for providing financial support through an INSPIRE Fellowship No. DST/INSPIRE Fellowship/2019/IF190871.

[1] Y. Kuramoto and D. Battogtokh, Nonlinear Phenom. Complex Syst. **5**, 380 (2002).
[2] D. M. Abrams and S. H. Strogatz, Phys. Rev. Lett. **93**, 174102 (2004).
[3] F. Parastesh, S. Jafari, H. Azarnoush, A. Shahriari, Z. Wang, S. Boccaetti, and M. Perc, Phys. Rep. **898**, 1 (2021).
[4] G. C. Sethia, and A. Sen, Phys. Rev. Lett. **112**, 144101 (2014).
[5] J. D. Hart, K. Bansal, T. E. Murphy, and R. Roy, Chaos **26**, 094801 (2016).
[6] C. R. Laing, Phys. Rev. E **92**, 050904(R) (2015).
[7] M. G. Clerc, S. Coulibaly, M. A. Ferríe, M. A. García-nustes, and R. G. Rojas, Phys. Rev. E **93**, 052204 (2016).
[8] C. Meena, K. Murali, and S. Sinha, Int. J. Bifurcation Chaos **26**, 1630023 (2016).
[9] H. Wang and X. Li, Phys. Rev. E **83**, 066214 (2011).

[10] V. K. Chandrasekar, J. H. Sheeba, B. Subash, M. Lakshmanan, and J. Kurths, Physica D **267**, 36 (2014).
[11] S. Ulonska, I. Omelchenko, A. Zakharova, and E. Schöll, Chaos **26**, 094825 (2016).
[12] A. zur Bonsen, I. Omelchenko, A. Zakharova, and E. Schöll, Eur. Phys. J. B **91**, 65 (2018).
[13] Y. Zhu, Z. Zheng, and J. Yang, Phys. Rev. E **89**, 022914 (2014).
[14] O. E. Omel'chenko, M. Wolfrum, S. Yanchuk, Y. L. Maistrenko, and O. Sudakov, Phys. Rev. E **85**, 036210 (2012).
[15] J. Xie, E. Knobloch, and H.-C. Kao, Phys. Rev. E **92**, 042921 (2015).
[16] Y. Maistrenko, O. Sudakov, O. Osiv, and V. Maistrenko, New J. Phys. **17**, 073037 (2015).
[17] N. S. Frolov, V. A. Maksimenko, V. V. Makarov, D. V. Kirsanov, A. E. Hramov, and J. Kurths, Phys. Rev. E **98**, 022320 (2018).
[18] S. Majhi, M. Perc, and D. Ghosh, Chaos **27**, 073109 (2017).
[19] L. Tumash, A. Zakharova, J. Lehnert, W. Just, and E. Schöll, Europhys. Lett. **117**, 20001 (2017).
[20] G. C. Sethia, A. Sen, and G. L. Johnston, Phys. Rev. E **88**, 042917 (2013).
[21] C. R. Laing, Physica D **238**, 1569 (2009).
[22] J. Xie, E. Knobloch, and H.-C. Kao, Phys. Rev. E **90**, 022919 (2014).
[23] S. W. Haugland, L. Schmidt, and K. Krischer, Sci. Rep. **5**, 9883 (2015).
[24] S. Thamizharasan, V. K. Chandrasekar, M. Senthilvelan, R. Berner, E. Schöll, and D. V. Senthilkumar, Phys. Rev. E **105**, 034312 (2022).
[25] T. Kapitaniak, P. Kuzma, J. Wojewoda, K. Czolczynski, and Y. Maistrenko, Sci. Rep. **4**, 6379 (2014).
[26] Y. Kuramoto and S. I. Shima, Prog. Theor. Phys. Suppl. **150**, 115 (2003).
[27] P. Ashwin and O. Burylko, Chaos **25**, 013106 (2015).
[28] M. J. Panaggio, D. M. Abrams, P. Ashwin, and C. R. Laing, Phys. Rev. E **93**, 012218 (2016).
[29] D. V. Senthilkumar and V. K. Chandrasekar, Phys. Rev. E **100**, 032211 (2019).
[30] Y. Maistrenko, S. Brezetsky, P. Jaros, R. Levchenko, and T. Kapitaniak, Phys. Rev. E **95**, 010203(R) (2017).
[31] N. M. Awal, D. Bullara, and I. R. Epstein, Chaos **29**, 013131 (2019).
[32] D. Dudkowski, K. Czołczynski, and T. Kapitaniak, Nonlinear Dyn. **95**, 1859 (2019).
[33] L. Larger, B. Penkovsky, and Y. Maistrenko, Nature Commun. **6**, 7752 (2015).
[34] J. Shena, J. Hizanidis, V. Kovanis, and G. P. Tsironis, Sci. Rep. **7**, 42116 (2017).
[35] J. Shena, J. Hizanidis, P. Hövel, and G. P. Tsironis, Phys. Rev. E **96**, 032215 (2017).
[36] C. Ramya, R. Gopal, R. Suresh, and V. K. Chandrasekar, Chaos **31**, 053113 (2021).
[37] A. Sharma, M. D. Shrimali, A. Prasad, R. Ramaswamy, and U. Feudel, Phys. Rev. E **84**, 016226 (2011).
[38] V. K. Chandrasekar, R. Gopal, A. Venkatesan, and M. Lakshmanan, Phys. Rev. E **90**, 062913 (2014).
[39] S. S. Chaurasia and S. Sinha, Nonlinear Dyn. **87**, 159 (2017).
[40] B. Ermentrout, *Simulating, Analyzing, and Animating Dynamical Systems: A Guide to XPPAUT for Researchers and Students* (SIAM, Philadelphia, 2002).
[41] A. Zakharova, M. Kapeller, and E. Schöll, Phys. Rev. Lett. **112**, 154101 (2014).
[42] K. Premalatha, V. K. Chandrasekar, M. Senthilvelan, and M. Lakshmanan, Chaos **28**, 033110 (2018).
[43] K. Sathiyadevi, V. K. Chandrasekar, and D. V. Senthilkumar, Phys. Rev. E **98**, 032301 (2018).
[44] D. M. Abrams, R. Mirollo, and S. H. Strogatz, and D. A. Wiley, Phys. Rev. Lett. **101**, 084103 (2008).
[45] R. Cestnik and A. Pikovsky, Phys. Rev. Lett. **128**, 054101 (2022).
[46] Y. Maistrenko, B. Penkovsky, and M. Rosenblum, Phys. Rev. E **89**, 060901(R) (2014).
[47] P. Jaros, Y. Maistrenko, and T. Kapitaniak, Phys. Rev. E **91**, 022907 (2015).
[48] P. Jaros, S. Brezetsky, R. Levchenko, D. Dudkowski, T. Kapitaniak, and Y. Maistrenko, Chaos **28**, 011103 (2018).
[49] E. Rybalova, V. S. Anishchenko, G. I. Strelkova, and A. Zakharova, Chaos **29**, 071106 (2019).
[50] F. Hellmann, P. Schultz, P. Jaros, R. Levchenko, T. Kapitaniak, J. Kurths, and Y. Maistrenko, Nature Commun. **11**, 592 (2020).